T-PAMI/9/6// 16848

# Error Analysis in Stereo Determination of 3-D Point Positions

S.D. Blostein
T.S. Huang

Reprinted from
IEEE TRANSACTIONS ON PATTERN ANALYSIS AND MACHINE INTELLIGENCE
Vol. PAMI-9, No. 6, November 1987

# Error Analysis in Stereo Determination of 3-D Point Positions

STEVEN D. BLOSTEIN, STUDENT MEMBER, IEEE, AND THOMAS S. HUANG, FELLOW, IEEE

*Abstract*—**The relationship between the geometry of a stereo camera setup and the accuracy in obtaining three-dimensional position information is of great practical importance in many imaging applications. Assuming a point in a scene has been correctly identified in each image, its three-dimensional position can be recovered via a simple geometrical method known as triangulation. The probability that position estimates from triangulation are within some specified error tolerance is derived. An ideal pinhole camera model is used and the error is modeled as known spatial image plane quantization. A point's measured position maps to a small volume in 3-D determined by the finite resolution of the stereo setup. With the assumption that the point's actual position is uniformly distributed inside this volume, closed form expressions for the probability distribution of error in position along each coordinate direction (horizontal, vertical, and range) are derived. Following this, the probability that range error dominates over errors in the point's horizontal or vertical position is determined. It is hoped that the results presented will have an impact upon both sensor design and error modeling of position measuring systems for computer vision and related applications.**

*Index Terms*—**Computer vision, image quantization effects, passive ranging, position error analysis, stereo image pairs, triangulation.**

## I. Introduction

A CRUCIAL task that faces computer vision and other triangulation systems is the ability to obtain accurate three-dimensional position information in the presence of limited sensor resolution. Sensors for computer processing applications produce sampled, quantized data whose spatial resolution is determined by limits in device technology and bandwidth. In computer vision and photogrammetry, a widely applicable passive ranging technique for obtaining 3-D data uses a stereo camera setup (Fig. 1). In finding the depth of a point in a scene, a triangulation must be performed on its projections onto two image planes. A knowledge of feature point correspondence is required to correctly match points in the image. Obtaining pairs of corresponding projection points is a difficult task and has received much attention in recent years [1], [6], [8]. Assuming correct point matches have already been identified, the next step is to recover the three-dimensional information via a simple geometrical method known as triangulation. Given a known quantization in image location (which may or may not correspond to the physical pixel size), the ensuing analysis will be concerned with the resulting position accuracy in triangulation for the case of two parallel image planes. Although accuracy in determining correspondence will depend upon the matching method used (complex features such as line intersections can produce subpixel accuracy), it is assumed that error modeling appropriate to the particular method of feature extraction may be equivalently expressed as a spatial quantization in the image planes. Within this assumption, the analyses presented here have application in robotics, autonomous vehicle navigation, photogrammetry, and radar.

Manuscript received April 21, 1986; revised May 21, 1987. Recommended for acceptance by R. Bajcsy. This work was supported in part by the National Science Foundation under Grant DCR-84-15325, and in part by Battelle Scientific Service Program under Contract DAAG29-81-D-0100.

The authors are with the Coordinated Science Laboratory, University of Illinois at Urbana-Champaign, Urbana, IL 61801.

IEEE Log Number 8716848.

### A. Existing Literature

Outside of the photogrammetry literature [14], the relationship between the geometry of the stereo camera setup and the accuracy in obtaining the actual 3-D positions has received scant attention though is of great practical importance. Duda and Hart [12] gives a brief treatment of the subject. McVey and Lee [2] have performed a worst case error analysis on the image plane resolution required to achieve depth measurement of a given accuracy. This problem has also been considered by Solina [15]. Recently, Verri and Torre's error analysis of depth estimates [16] separated the errors into two components. The first, precision of the setup geometry, affects absolute depth estimates while the second, image plane orientation and focal length/image separation ratio, affects relative depth estimates. In some cases, triangulation is not performed explicitly: a linear relationship between the 2-D and 3-D coordinates is expressed through a 4 by 3 projective matrix [12], [14], [17] determined by a camera calibration procedure. For the construction of accurate depth maps, [1], [6], [9], or the estimation of motion parameters from 3-D data obtained by a sequence of stereo pairs of images [3]–[5], [7], [10], [17], the resolution requirement is severe and a conservative worst case design is not feasible. Thus, to live within the constraints of limited spatial resolution, a greater understanding of position error from image plane *quantization* is crucial.

### B. Problem Definition

A much more useful alternative to the worst case analyses such as in [2] and [14] would be to determine the *probability* that a certain position estimate is within a specified position tolerance given the camera geometry of

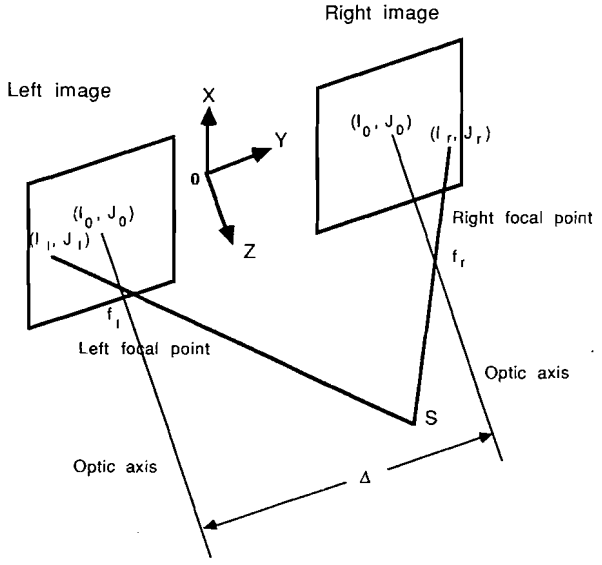


Fig. 1. Stereo camera setup.

a stereo setup. It seems that such an approach is not taken in the photogrammetry literature (see [14] for references). As attempted in [14], this paper analyses the accuracy in obtaining 3-D position of *points* by triangulation on two quantized image planes. It will be assumed that the only cause of error is image plane quantization in terms of a system of image coordinates. A *pinhole* camera model [9] is used thus ignoring camera lens distortion and other optical nonlinearities. Despite these simplifications, results presented are quite general in that they are lower bound performance estimates for any imaging systems that process sampled image data. A further assumption is a limitation of the possible camera geometries; the left and right cameras are at equal height and orientation, i.e., the coordinate axes of the two image planes are related by a horizontal shift in position. This camera geometry has important practical applications since the search for image point "correspondences" can then be restricted to searching a single scan line. Moreover, the parallel camera geometry is used in instances where the recovery of rather large depth values is critical. This restriction in camera geometry, then, still applies to many stereo setups of interest.

### C. Scope of the Analysis

The analysis that follows will help quantify several major observations about obtaining 3-D point positions via a triangulation procedure:

1) On the general assumption that the exact unknown 3-D point location lies *uniformly* anywhere within a small volume around its true position, the probability distribution of the error in position measurement along each of the coordinate axes will be derived.

2) The degree to which the error in estimating perpendicular distance from the image planes (range) dominates over errors in measuring the point's horizontal or vertical position will be quantified.

## II. Setup

### A. Linear Pinhole Model Assumption

Before describing the stereo setup we will first look more closely at the effects of a major simplifying assumption made in Section I-B to further ascertain the applicability of the analysis. Recall that a *pinhole* camera model is employed for each camera. That is, the lens is considered to be a point through which all incoming rays of light pass. Simple geometric optics reveal that such a camera can focus perfectly on all points in the camera's field of view. In reality, a pinhole cannot be used since it does not allow enough light through to the imaging surface. For this reason, a lens is used whose aperture size is set to be inversely proportional to the amount of light in the scene. However, this finite aperture allows only one range (distance along the optic axis) to be focused upon exactly, while all other depths have an associated *circle of confusion* in the image plane [9]. One may assume that in well-lighted conditions and with a proper geometrical setup, the lens aperture is small enough so that the effect of such blurring is small compared to the camera's other distortions. Under such conditions a pinhole model can be accepted as a very close approximation to a lens' behavior.

### B. Triangulation in the Case of Parallel Image Planes

A simple mathematical expression for a point's 3-D coordinates in terms of the two sets of quantized image coordinates and the parallel projection camera geometry will be presented (for a similar approach, see [13]). With the two image planes at the same height, a point in 3-D is projected onto the same horizontal scan line in each of the two images. Illustrated in Fig. 1 is the geometry to be used for such a setup. The points $f_l$ and $f_r$ are the focal points of the left and right cameras. The quantities $dv$ and $du$ are, respectively, the horizontal and vertical pixel spacings of the two imaging surfaces. $\Delta$ denotes the distance between the two optical axes and is usually referred to as the *baseline* of the system. A point $S$ on the object will have coordinates $(x, y, z)$. For image pixel coordinates, let (0, 0) be at the center of each image, through which the optical axis passes. These image coordinate system origins are depicted in Fig. 1 as $(I_0, J_0)$. The coordinates of $S$'s projections on the imaging surfaces are as follows: as shown in Fig. 1, point $S$ projected onto the left imaging surface will have coordinates $(I_l, J_l)$ where each coordinate ranges from $-N/2$ to $N/2 - 1$ pixels for a resolution of $N$ by $N$ pixels. Similarly, $S$ will be projected onto $(I_r, J_r)$ in the right image. As defined above, references to the right and left images will be distinguished by subscripts "$l$" and "$r$."

Due to the camera geometry described, the vertical coordinate will be the same in both images, i.e., $I_l = I_r$. In a 3-D *world* coordinate system with origin at point "O" midway between the two image centers, a point at $(I_l, J_l)$ would lie at $(I_l du, -\Delta/2 + J_l dv, 0)$. From Fig. 1 it is easy to derive the location of $S$ in terms of the coordinates $(I_l, J_l)$ and $(I_r, J_r)$ and camera parameters: $f$, the common

focal length, $\Delta$, the baseline distance, and $dv$, the pixel dimension. This operation is simply known as *triangulation* and can be performed by the use of similar triangles. From Fig. 1, point

$$S(x, y, z) = \left[\frac{\Delta I_l}{(J_r - J_l)}, \Delta\left(\frac{1}{2} + \frac{J_r}{J_r - J_l}\right), \frac{\Delta f}{(J_r - J_l)\, dv} + f\right] \quad (1)$$

assuming $du = dv$. From (1), the location of point $S$ can be found in terms of imaged $I_l$, $I_r$, $J_l$, $J_r$ and known $f$, $dv$, and $\Delta$. It is assumed that both cameras have the same focal length $f$. The assumption $du = dv$ is without loss of generality, for the convenience of simplifying expressions in the analysis that follows.

## III. Stereo Quantization

### A. True versus Sampled Projection Point Positions

An implicit assumption made in (1) is that $S$ projects exactly onto the integer valued image coordinates. However, the exact location of the projection onto the left image, for example, is not at coordinates $(I_l, J_l)$, but within $(I_l \pm \frac{1}{2}, J_l \pm \frac{1}{2})$. A sampled imaging system locates a projected point no more accurately than within the nearest integer pixel coordinates. We can define the actual locations of the left and right horizontal components of the projections on the image in our 3-D system as

$$y_l \equiv \left(-\frac{\Delta}{2} + \left(J_l + n_l - \frac{1}{2}\right) dv\right) \quad (2a)$$

$$y_r \equiv \left(\frac{\Delta}{2} + \left(J_r + n_r - \frac{1}{2}\right) dv\right) \quad (2b)$$

where $n_l$ and $n_r$ are real numbers between 0 and 1. In Fig. 2 a horizontal "slice" of the 3-D space in Fig. 1 is shown. Similar definitions to (2a) and (2b) can be given for the vertical $(x)$ projection. Due to the *parallel projection* camera geometry assumed for this problem it can be observed in (1) that the locations of the $y$ and $z$ positions of any 3-D point are functions of only the horizontal $(J)$ coordinates and are independent of vertical image position $(I)$. As a consequence, an analysis of the accuracy in locating the $y$ or $z$ components of a 3-D point can be carried out simply by considering any one of an infinite number of identical (horizontal) $y$–$z$ plane slices of the 3-D space pictured in Fig. 2.

### B. Uncertainty in 3-D Position Due to Image Quantization

By inspection of (2) the uncertainty in locating a 3-D point comes from the quantities $n_l$ and $n_r$ not being physically obtainable for any finite resolution system: there will be an uncertainty of $\pm\frac{1}{2}$ pixel for any pixel size. This uncertainty can be viewed as a *stereo quantization process* where $n_l = n_r = \frac{1}{2}$. The expression reduces to (1) where $S$ is observed with integer valued $I$ and $J$ coordinates. To quantify the amount of uncertainty involved in the location of a 3-D point from stereo vision we assume no *a priori* information about its true position. Referring to Fig. 2, the projection of the 3-D space in the $y$–$z$ (horizontal and depth) plane, we assume that the actual location of a point can be anywhere within quadrilateral $P1$, $P2$, $P3$, $P4$ (since $n_l$ and $n_r$ are unknown). In other words, the observed horizontal coordinate $J_r$ arises from the true location of a point which we will assume to be within $P1$, $P2$, $P3$, $P4$ with equal probability.

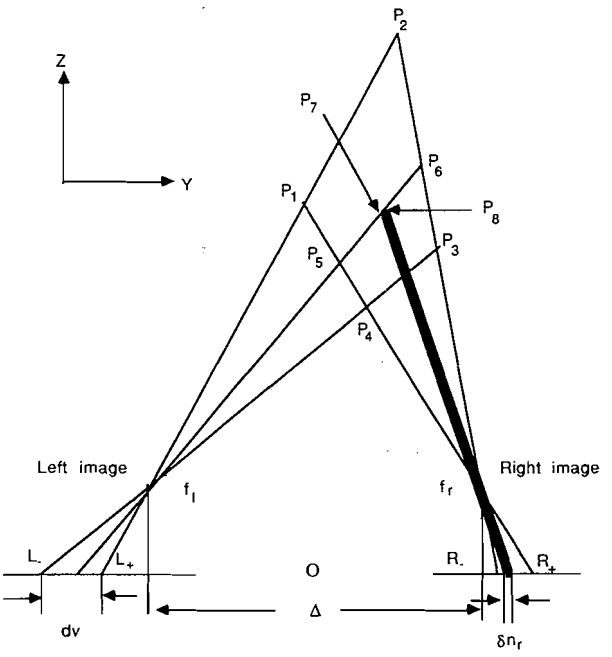


Fig. 2. Horizontal projection of a triangulation.

### C. Geometry of Horizontal ($y$–$z$) Slice of Region of Uncertainty

Let us assume that the point $S$ may lie *with uniform distribution* within the quadrilateral $P1$, $P2$, $P3$, $P4$, which we denote as the *region of uncertainty*, or ROU. More generally, $S$ can lie uniformly within some volume due to additional uncertainty in the vertical coordinate. Fig. 2 depicts the $y$–$z$ projection of such a region of uncertainty.

In order to proceed further, expressions for the length of segments $\overline{P5P6}$ and $\overline{P7P8}$ in Fig. 2 must be derived in terms of the unknowns $n_l$ and $n_r$. In Appendix A, expressions for the segments' end points are determined and approximations for their lengths are obtained. Following this, a statistical interpretation of the projection points is given using simple geometric reasoning about these segment lengths. From Appendix A, (A1), segment $\overline{P5P6}$ (Fig. 2) has, to a close approximation, length

$$\|P5 - P6\| \approx \frac{\Delta}{(J_l - J_r + n_l)(J_l - J_r + n_l - 1)} \cdot \left[\frac{f^2}{dv^2} + J_l^2\right]^{1/2}. \quad (3)$$

Also from Appendix A, (A2), the length of the projection

of an infinitesimally thin interval of width $dn_r$ in the image plane upon segment $\overline{P5P6}$, $\overline{P7P8}$, can be approximated to second order by

$$\| P7 - P8 \| \approx \frac{\Delta dn_r}{(J_l - J_r + n_l - n_r)^2} \left[ \frac{f^2}{dv^2} + J_l^2 \right]^{1/2}. \quad (4)$$

## IV. Statistical Interpretation of Projection Points

From (1), uncertainty in range ($z$) and horizontal position ($y$) are purely a result of quantization in the horizontal ($J$) coordinate and are independent of the vertical ($I$) coordinate. An analysis of triangulation can proceed by first considering a horizontal slide ($y$–$z$) of the 3-D space and the associated horizontal component of the image planes. From here on consider a *horizontal slice* of the 3-D space. Assume that a point in $y$–$z$ space may lie anywhere uniformly within the ROU in Fig. 2. This model of the uncertainty is reasonable since *a priori* information about the point's position within the ROU ($P1$, $P2$, $P3$, $P4$) does not exist. This is where the probabilistic model of the problem originates, resulting in a probabilistic interpretation of $n_l$ and $n_r$ as continuous random variables, $N_l$ and $N_r$.

The analysis is summarized as follows: the distributions are found from the projection of the ROU onto a horizontal line in each of the image planes. The probability that $N_l$ takes on a value $n_l$ can be modeled as being proportional to the area of a very thin rectangle with length $\| P5 - P6 \|$ and infinitesimal width. Since the point in Fig. 2 lies anywhere uniformly in the region bounded by $P1$, $P2$, $P3$, $P4$, it has a greater probability in being projected onto an $n_l$ that corresponds to a longer segment $\overline{P5P6}$. The second step is to derive the conditional density of $n_r$ given that $S$ projects onto $n_l$. This is just proportional to the length on $\overline{P5P6}$, $\| P7 - P8 \|$, that an infinitesimally thin segment in the right image, $\delta n_r$, will project. In places along $n_r$ where $\delta n_r$ projects onto a longer segment $\overline{P5P6}$, point $P$ will be found inside this larger area with a correspondingly higher probability. From the density of $N_l$ and the conditional density of $N_r$, given $N_l$, the joint density of $N_l$ and $N_r$ is straightforwardly obtained.

### A. Joint Probability Distribution of Projection Points

With a point uniformly distributed in the ROU, the marginal density of the projection of such a point onto the left image plane is simply proportional to the length of segment $\overline{P5P6}$ corresponding to a projection point, $n_l$, located between $L_-$ and $L_+$. This can be thought of as the ratio of the area swept out by a thin strip bounded by $\overline{P5P6}$ to the area of the ROU. Expressing the line segment length $\| P5 - P6 \|$ (3) as a probability measure of $n_l$, we get the density

$$f_{N_l}(n_l) = \frac{\left[ \frac{1}{(J_l - J_r + n_l - 1)} - \frac{1}{(J_l - J_r + n_l)} \right]}{-\ln \left| 1 - (J_r - J_l)^{-2} \right|} \quad 0 \le n_l \le 1. \quad (5)$$

Once it is known that a point projects onto $n_l$ in the left image, the projection on the right image is constrained by the fact that the point lies somewhere on $\overline{P5P6}$ in the ROU. Since $\overline{P5P6}$ has a different slope depending on $n_l$, the point is projected differently on the right image depending on the value of $n_l$. The probability density is proportional to the length of the projection that a very thin strip $dn_r$ makes on $\overline{P5P6}$ as a function of the position along the interval $[R_-, R_+]$. This quantity is simply the segment $\overline{P7P8}$ (4). By normalizing $\| P7 - P8 \|$ to be a probability measure of position along $[R_-, R_+]$, or, equivalently, as a function of the value of $n_r$, the conditional distribution obtained is

$$f_{N_r | N_l}(n_r \mid n_l) = \frac{\frac{1}{(J_l - J_r + n_l - n_r)^2}}{\frac{1}{J_l - J_r + n_l - 1} - \frac{1}{J_r - J_l + n_l}}.$$

The *joint density* [11] of the distribution on the two image planes is

$$f_{N_l, N_r}(n_l, n_r) = f_{N_r | N_l}(n_r \mid n_l) f_{N_l}(n_l).$$

Multiplying the previous derived expressions gives

$$f_{N_l, N_r}(n_l, n_r) = \frac{1}{-\ln \left| 1 - (J_r - J_l)^{-2} \right| (J_l - J_r + n_l - n_r)^2} \quad (6)$$

where $0 \le n_l \le 1$, $0 \le n_r \le 1$.

## V. Analysis of Position Errors

### A. Probability that Error in Range (z) Less than a Specified Tolerance

From the joint density derived in (6), probabilities of various events involving the random variables $N_l$ and $N_r$ can be determined by integration over an appropriate region. For example, the joint probability distribution of the projection points of the ROU on the left and right image planes can be directly used to derive the uncertainty in ranging a point using triangulation. Define the relative error in ranging a point as

$$\epsilon_z = \frac{\hat{z} - z}{z} \quad (7)$$

where $z$ is the exact range of the point,

$$z = \frac{f\Delta}{dv}\left[\frac{1}{(J_r - J_l + n_r - n_l)}\right] \tag{8}$$

and $\hat{z}$ is the quantized ranged point,

$$\hat{z} = \frac{f\Delta}{dv}\left[\frac{1}{(J_r - J_l)}\right]. \tag{9}$$

From here on we define the *disparity* $D \equiv J_r - J_l$. Note that the quantization process assigns the values $\frac{1}{2} = n_r = n_l$. Substituting (8) and (9) into (7) gives

$$\epsilon_z = \frac{n_l - n_r}{J_r - J_l}. \tag{10}$$

The probability of the range value being within a certain tolerance $\tau_z$ can now be formulated as

$$P(|\epsilon_z| < \tau_z) = P\left(-\tau_z < \frac{n_l - n_r}{J_r - J_l} < \tau_z\right).$$

The task is now to integrate the joint density of $N_l$ and $N_r$ given by (6) in the region of the $n_l - n_r$ plane defined by the above equation which can be further manipulated to yield a square region above the plane bounded by two slanted parallel lines:

$$P(|\epsilon_z| < \tau_z) = P(-\tau_z(J_r - J_l) + n_r < n_l < \tau_z(J_r - J_l) + n_r).$$

Examination of the $n_l - n_r$ plane reveals that this expression is equivalent to the unit volume over the entire region minus the volume of the regions above and below the parallel lines, or

$$1 - \int_{\tau_z(J_r - J_l)}^{1} \int_{0}^{n_r - \tau_z(J_r - J_l)} f_{N_l,N_r}(n_l, n_r)\, dn_l dn_r - \int_{\tau_z(J_r - J_l)}^{1} \int_{0}^{n_l - \tau_z(J_r - J_l)} f_{N_l,N_r}(n_l, n_r)\, dn_r dn_l.$$

The integration of this joint density (6) within the above region yields

$$P_{|\epsilon_z|}(|\epsilon_z| < \tau_z) = \begin{cases} \dfrac{1}{\ln(1 - D^{-2})}\left(\dfrac{2\tau_z(\tau_z - D^{-1})}{1 - \tau_z^2} + \ln(1 - \tau_z^2)\right) & \tau_z < \dfrac{1}{D} \\ 1 & \tau_z \geq \dfrac{1}{D} \end{cases} \tag{11}$$

where $\tau_z$ is the relative error in ranging point $S$ and $D \equiv J_r - J_l$ is the horizontal pixel difference between the left and right images. Note that the above expression only depends upon the disparity $D$ associated with point $S$.

*1) First Order Approximation and Comparison to (11):* It turns out that (11), the derived probability expression for error in range, can be simplified greatly without appreciable loss in accuracy as long as the error disparity exceeds several pixels (as in most practical cases). We use the first order Taylor series approximation of the "logarithm" terms in (11),

$$\ln(1 - D^{-2}) \approx -D^{-2} \tag{12a}$$

$$\ln(1 - \tau_z^2) \approx -\tau_z^2. \tag{12b}$$

Substituting these into (11) yields the approximate expression

$$\hat{P}_{|\epsilon_z|}(|\epsilon_z| < \tau_z) \equiv \begin{cases} 1 - (1 - \tau_z D)^2 & \tau_z < \dfrac{1}{D} \\ 1 & \tau_z \geq \dfrac{1}{D}. \end{cases} \tag{13}$$

Recall that the only assumption made in the derivation of (11) is that $S$ may lie uniformly within a volume in 3-D whose horizontal projection is the region of uncertainty in Fig. 2. Suppose we instead assume that $N_l$ and $N_r$ are independent and uniformly distributed between 0 and 1. Their joint density would then be uniform. It can be shown that the resulting distribution of range error would be identical to (13). Finally note that the density function of range error, the derivative of (13), is highly non-Gaussian: it is defined over a finite interval and has a constant slope.

The degree to which (13) approximates (11) must now be quantified. In Appendix B it is shown that the maximum error over all $\tau_z$ between the two probability distribution functions (13) and (11) is

$$\underset{\tau_z}{\operatorname{argmax}} \left| P_{|\epsilon_z|}(\tau_z) - \hat{P}_{|\epsilon_z|}(\tau_z) \right| < \frac{D^2}{D^4 - 1}. \tag{14}$$

For example, if the disparity, $D = 10$ pixels, the maximum distance over $\tau_z$ between (11) and (13) is less than 0.01. This explains the use of the same dashed line for the two functions (plotted in Fig. 3, where $D = 50$ and the maximum distance is within 0.004. Note that for small $D$, (13) may have significant inaccuracy and (11) must instead be used. However, for the purposes of the remaining discussion, we will use (13) as an adequate approximation.

*2) Experimental Verification:* A computer simulation was performed in order to verify the derived range error distribution of (11) as well as its approximation (13). An ideal pinhole camera model of the stereo setup was used to project randomly generated uniformly distributed points in 3-D onto two parallel planes. For all experiments described in this paper, the camera geometry consisted of two identical 512 by 512 pixel resolution imaging surfaces of dimension 50.8 mm ($dv$) by 38.1 mm ($du$). The baseline distance between optical axes was 0.5 meters and the focal length of each camera was 28 mm, corresponding to a 75° view angle.

The purpose of the experiment was to verify the cumulative distribution functions of (11) and (13). A large

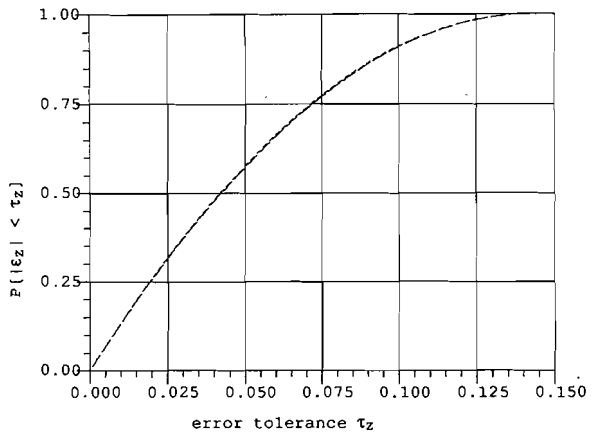


Fig. 3. Cumulative distribution function of relative error in range for a disparity, $D = 50$. The dashed line is the theoretical value (13), while the solid line is the experimentally determined edf.

number of points in 3-D were generated randomly so as to be visible to the simulated stereo setup. A pair of quantized image coordinates were generated for each 3-D point. The observed location of the point was determined by performing a triangulation on these integer-valued coordinates. The error was calculated as the absolute value of (7). Fig. 3 plots the cumulative distribution function (cdf) for points that have a disparity of 50 pixels. It turns out that (13) is an extremely good approximation for (11) and both error expressions represent the same dashed line on the plot. The solid line is the experimentally determined cdf of $|\epsilon_z|$. In the experiment, several hundred points produced the histogram shown. On the horizontal axis is the relative error in range $\tau_z$, while the vertical axis represents the probability that $|\epsilon_z|$ does not exceed this tolerance. As shown in Fig. 3, the theoretical results echo the experimental findings quite closely.

### *B. Probability of Horizontal Position (y) Error Less than a Specified Tolerance*

In a similar fashion, the probability distribution for position errors in the horizontal ($y$) direction is now derived. First, we let $y$ denote the true horizontal position of an imaged point and $\hat{y}$ denote the measured horizontal position found from triangulation. Thus

$$y = \Delta\left[\frac{J_r + n_r - \frac{1}{2}}{J_r - J_l + n_r - n_l} + \frac{1}{2}\right] \tag{15a}$$

$$\hat{y} = \Delta\left[\frac{J_r}{J_r - J_l} + \frac{1}{2}\right]. \tag{15b}$$

For convenience we let $h \equiv J_r$, if $J_r \neq 0$, be a horizontal pixel deviation (note that $h > 0$), we let $D \equiv J_r - J_l$, the disparity, and $R \equiv f/dv$, the *resolution factor*. The error, then, as a function of depth is

$$\epsilon_y = \frac{\hat{y} - y}{z} = \frac{1}{R}\left[\frac{h(D + n_r - n_l)}{D} - h - n_r + \frac{1}{2}\right]. \tag{16}$$

The calculation consists of determining an expression for $P(|\epsilon_y| < \tau_y)$ where $\tau_y$ is a positive valued error tolerance. From the above definitions.

$$\begin{aligned} &P(-\tau_y < \epsilon_y < \tau_y) \\ &\quad = P\left(\frac{D}{h}\left(\frac{1}{2} - R\tau_y\right) + (1 - D/h)\, n_r < n_l \right. \\ &\qquad \left. < \frac{D}{h}\left(\frac{1}{2} + R\tau_y\right) + (1 - D/h)\, n_r\right) \end{aligned} \tag{17}$$

which must be integrated over the appropriate region of the $n_r - n_l$ plane. Unfortunately, such an integration is much more complicated than that performed in the derivation of range error distribution (11). It will be assumed that the joint distribution of $n_l$ and $n_r$ will have constant unit value as approximated in Section V-A-1). Note that (17) reveals a region bounded by parallel lines in the $n_r - n_l$ plane having a separation and slope dependent on the quantities defined. This region intersects a square consisting of realizable values of $n_l$ and $n_r$ in many different ways. It can be shown that the integration of (17) yields the following expression:

let

$$\operatorname{sgn}(x) = \begin{cases} 1 & x \geq 0 \\ -1 & x < 0 \end{cases}$$

$$A = \frac{2DR\tau_y}{\max(h, D - h)}$$

$$B = \frac{D^2\left(\frac{1}{4} + R^2\tau_y^2 + \operatorname{sgn}(h - D)\, R\tau_y\right)}{h(D - h)}.$$

In terms of the quantities defined above,

$$P(-\tau_y < \epsilon_y < \tau_y)$$

$$= \begin{cases} A & 0 \leq \tau_y < \frac{1}{R}\left|\frac{1}{2} - \frac{h}{D}\right| \\ 1 - B & \frac{1}{R}\left|\frac{1}{2} - \frac{h}{D}\right| \leq \tau_y < \frac{1}{2R} \\ \quad \text{if } 0 \leq h < D & \\ 1 & \tau_y \geq \frac{1}{2R} \end{cases}$$

$$\cdot \begin{cases} A & 0 \leq \tau_y < \frac{1}{2R} \\ B - A \operatorname{sgn}(h - D) & \frac{1}{2R} \leq \tau_y < \frac{1}{R}\left|\frac{1}{2} - \frac{h}{D}\right| \\ \quad \text{otherwise} & \\ 1 & \tau_y \geq \frac{1}{R}\left|\frac{1}{2} - \frac{h}{D}\right|. \end{cases}$$

(18)

Note that the above function is symmetrical about $h =$

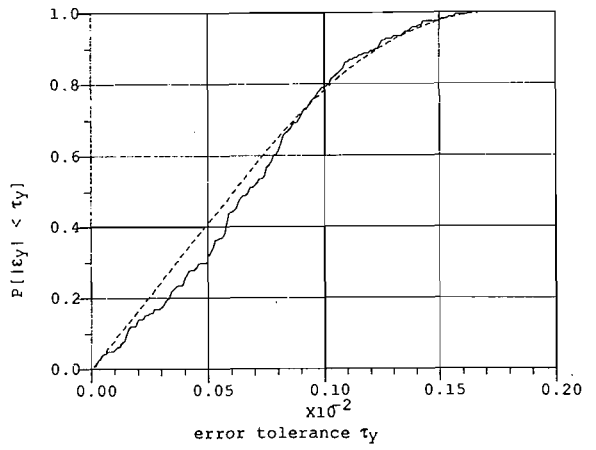


(a)

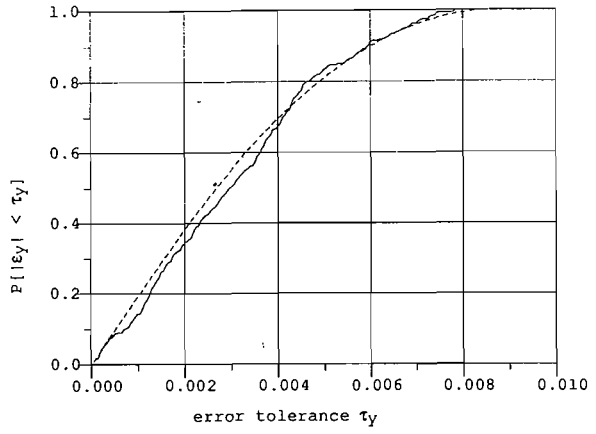


(b)

Fig. 4. Cumulative distribution function of error in horizontal position for a disparity of 50 pixels and horizontal displacement of (a) 35 pixels and (b) 150 pixels. Dashed line is from (18), solid line is the experimentally determined cdf.

$D/2$, a plane equidistant from the two focal points. Even though the triangulation calculation is asymmetrical with respect to the left and right images, the resulting error distribution is symmetrical. As a result, the error distribution is invariant to the two possible ways that the triangulation calculation may be performed (an expression equivalent to (1) may be derived for the "$y$" coordinate based on $J_l$ rather than $J_r$).

*1) Experimental Verification:* A computer simulation was used to verify (18), the cumulative distribution function. The same stereo setup was used as in the range error experiment of the previous section. The same procedure was adopted [see Section V-A-2)] in the random point selection and quantization. In this experiment, however, additional information was recorded: the horizontal pixel displacement from the center of the right image plane, $h$. The resolution factor, $R = f/dv = 28.0 \times 512/50.8$. Fig. 4(a) shows the cumulative distribution function for a disparity $D$ of 50 pixels and horizontal displacement $h$ of 35 pixels. The dashed line is a plot of (18) while the solid line is the experimentally determined cdf based on about 200 calculated samples of the error $|\epsilon_y|$. Fig. 4(b) shows a similar plot where $h = 150$ pixels. This latter case represents a point nearer to the edge of the image plane whereas Fig. 4(a) is the error distribution of a point near the center of the image plane. Note the higher probability of error in the case $h = 150$ pixels.

### *C. Probability of Vertical Position ($x$) Error Less than a Specified Tolerance*

The positional error distribution for the vertical ($x$) direction is now derived. Unlike the range and horizontal directions, which are functions of only the random variables $N_r$ and $N_l$, the vertical position error is also a function of quantization in the vertical as well as the horizontal direction. Analogous to horizontal image coordinates $J_r$ and $J_l$, with respective error components $n_r$ and $n_l$, we can define

$$x_l \equiv x_r \equiv (I_l + n_v - \tfrac{1}{2})\, du \tag{19}$$

where $n_v$ is the subpixel uncertainty in vertical position (ranging from 0 to 1), and $du$ is the vertical pixel spacing. Note that for the stereo setup considered, $I_l = I_r$. Without loss of generality we will assume $du = dv$ to avoid carrying around the extra constants. The formulation proceeds as usual where the error expression

$$\epsilon_x = \frac{(\hat{x} - x)}{z} \tag{20}$$

and $\hat{x}$ is the vertical position found from triangulation while $x$ is the true vertical position. Using (1),

$$x = \frac{\Delta(I + n_v - \frac{1}{2})}{(J_r - J_l + n_r - n_l)}$$

while for the quantized point,

$$\hat{x} = \frac{\Delta I_l}{(J_r - J_l)}.$$

Substitution into (20) gives the error expression

$$\epsilon_x = \frac{1}{R}\left[\frac{v(D + n_r - n_l)}{D} - \left(v + n_v - \frac{1}{2}\right)\right] \tag{21}$$

where $v \equiv I_l$, if $I_l \neq 0$, is a nonzero vertical pixel displacement from the image center and $D$ is the disparity. Without loss of generality we will consider the case where $v > 0$ since there is symmetry about the horizontal plane passing through the focal points of the cameras. Using (21) and simplifying the right-hand side yields

$$P(|\epsilon_x| < \tau_x) = P\left(-\frac{RD}{v}\tau_x - \frac{D}{2v} < n_r - n_l - \frac{D}{v}n_v < \frac{RD}{v}\tau_x - \frac{D}{2v}\right). \tag{22}$$

As in Section V-A-1), the random variables $n_r$ and $n_l$ will be taken to be independent and uniformly distributed, defined on [0, 1). The random variable $n_v$, representing vertical image quantization, is independent of the other two quantities and is also uniform on [0, 1). This follows

from the assumed uniform distribution for the position uncertainty and the parallel projection camera model removing the dependency between vertical and horizontal spatial quantization.

With distributions now specified for the random variables $n_r$, $n_l$, and $n_v$, their joint distribution can trivially be specified as a uniform density unit cube,

$$f_{n_v,n_l,n_r} = \begin{cases} 1 & 0 \le n_v \le 1,\ 0 \le n_l \le 1,\ 0 \le n_r \le 1 \\ 0 & \text{otherwise.} \end{cases} \tag{23}$$

Integration of (22) in the cube region of (23) is the final step to obtain the probability distribution. Examination of (22) reveals the unit cube cut by two parallel planes that may intersect in many possible orientations depending upon image plane location, camera model parameter values, and maximum error tolerance parameter $\tau_x$.

$$P(|\epsilon_x| < \tau_x) = \int_0^1 \int_0^1 \int_{\max[0,(v/D)(n_r-n_l)-R\tau x+1/2]}^{\min[1,(v/D)(n_r-n_l)+R\tau x+1/2]} dv_v\, dn_l\, dn_r. \tag{24}$$

The computational problem arises from the limits of the integral with respect to $n_v$, expressed as minimum and maximum functions of the variables $n_r$ and $n_l$. Obtaining a closed form expression for (24) involves dividing up the triple integral into a large number of cases (26 in all) each representing a region of integration applicable to different relative magnitudes of the variables $D$, $v$, $R$, and $\tau_x$. Since the cumulative distribution function of $\tau_x$ is of interest, the resulting expression is in the form of a piecewise continuous function of $\tau_x$. Thus, the integration turns out to be a rather tedious exercise due to a large amount of "case chasing." The mathematical software package MACSYMA was used to symbolically evaluate the 26 triple integrals. This results in the following distribution for $\tau_x$:

Let

$$\phi = -\frac{v}{3D} - \frac{DR^2\tau_x^2}{v} + \frac{DR\tau_x}{v} - \frac{D}{4v} + R\tau_x$$

$$\psi = \frac{D^2R^3\tau_x^3}{3v^2} - \frac{D^2R^2\tau_x^2}{2v^2} + \frac{D^2R\tau_x}{4v^2} - \frac{D^2}{24v^2}$$

$$\rho = \frac{2DR\tau_x}{v} - \frac{2D^2R^3\tau_x^3}{3v^2} - \frac{D^2R\tau_x}{2v^2}$$

$$\theta = -\frac{3D^2R\tau_x}{4v^2} + \frac{5D^2}{24v^2} - \frac{1}{2}.$$

In terms of the quantities defined above,

$$P(-\tau_x < \epsilon_x < \tau_x) = \begin{cases} 1 & \tau_x > \dfrac{v}{DR} + \dfrac{1}{2R} \\ \phi + \theta & \dfrac{v}{2DR} + \dfrac{1}{2R} < \tau_x \le \dfrac{v}{DR} + \dfrac{1}{2R} \\ \phi + \Psi + \dfrac{1}{2} & \dfrac{1}{2R} < \tau_x \le \dfrac{v}{2DR} + \dfrac{1}{2R} \\ \phi - \Psi + \dfrac{1}{2} & -\dfrac{v}{DR} + \dfrac{1}{2R} < \tau_x \le \dfrac{1}{2R} \\ 2R\tau_x & 0 \le \tau_x \le -\dfrac{v}{DR} + \dfrac{1}{2R} \quad \text{and} \quad D \ge 2v \\ \rho & 0 \le \tau_x \le -\dfrac{v}{DR} + \dfrac{1}{2R} \quad \text{and} \quad D < 2v \end{cases} \quad \text{if } D \ge v$$

$$\begin{cases} 1 & \tau_x > \dfrac{v}{DR} + \dfrac{1}{2R} \\ \phi + \Psi + \dfrac{1}{2} & \dfrac{v}{DR} - \dfrac{1}{2R} < \tau_x \le \dfrac{v}{DR} + \dfrac{1}{2N} \\ \dfrac{2DR\tau_x}{v} - \dfrac{D^2R^2\tau_x^2}{v^2} - \dfrac{D^2}{12v^2} & \dfrac{1}{2R} < \tau_x \le \dfrac{v}{DR} - \dfrac{1}{2R} \\ \rho & 0 \le \tau_x \le \dfrac{1}{2R} \end{cases} \quad \text{else.} \tag{25}$$

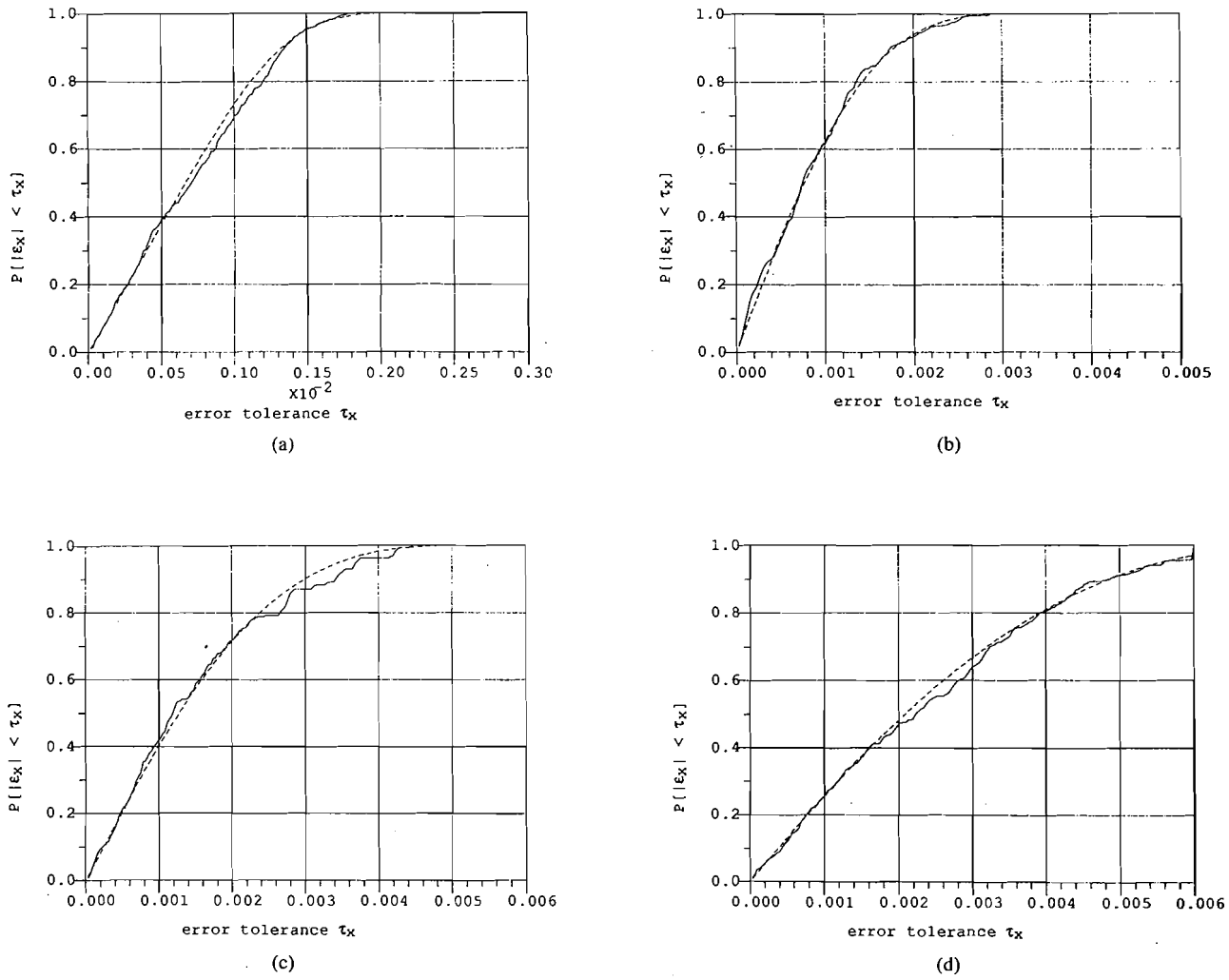


Fig. 5. Cumulative distribution function of error in vertical position for a disparity of 50 pixels and vertical displacement of (a) 15, (b) 35, (c) 75, and (d) 130 pixels. Dashed line is from (25), solid line is the experimentally determined cdf.

The lengthy details of this calculation have been omitted. Note that the symmetric case where $v < 0$ can be handled in likewise manner yielding an identical set of expressions.

*1) Experimental Verification:* Evidence for the correctness of the vertical positional error probability distribution expressions has been obtained by performing a computer simulation using the stereo setup and pinhole camera model described. A disparity $D$ of 50 pixels was used and four different values of $v$ were tried corresponding to four different cases of (25): a) ($v = 15$), b) ($v = 35$), c) ($v = 75$), d) ($v = 130$). 3-D points were randomly chosen and quantized according to the camera model. For each point that had the same selected $D$ and $v$, $|\epsilon_x|$ was calculated and the resulting collection of error points was histogrammed and was compared to the theoretical distribution predicted by (25). This is shown in Fig. 5(a)–(d). Each experimental cdf (solid line) is based on several hundred random points that were projected into the ROU corresponding to the four respective image locations. Note the closeness of the experimental and analytical results. Also, note the increase in error from cases (a) to (d), as the points are located closer to a vertical edge of the image plane.

Probability distributions have now been derived for position errors (as a fraction of range error) in each coordinate direction: range ($z$) in Section V-A horizontal ($y$) in Section V-B, and vertical ($x$) in this section. The next step is to find ways of quantitatively comparing these distributions, the subject of the next section.

### *D. Error in Range Dominates over Vertical Position Error*

In this section, the degree to which the error in range ($z$) dominates over the vertical ($x$) error will be explored. We start off by substituting the expression for $\epsilon_z$ (10), into the expression for the error in the $x$ component, i.e., we write $\epsilon_x$ as a function of $\epsilon_z$:

$$\epsilon_x = \frac{1}{R} v\epsilon_z + \frac{-n_t + 1/2}{R}. \tag{26}$$

Using the Triangle Inequality, $\epsilon_x$ can be bounded from

below:

$$|\epsilon_x| \leq \left|\frac{1}{R} v\epsilon_z\right| + \left|\frac{n_v - 1/2}{R}\right|$$

or

$$|\epsilon_x| \leq \frac{1}{R} v|\epsilon_z| + |B| \tag{27}$$

where $B \equiv 1/R\,|n_v - \frac{1}{2}|$ is a random variable uniformly distributed on $[-1/2R, 1/2R]$, independent of $\epsilon_z$ [by the same argument which lead to (23)]. Next, the quantity $P(B \leq \alpha|\epsilon_z|)$, for some positive constant $\alpha$, must be determined. The details of this calculation are found in Appendix C:

$$P(B \leq \alpha|\epsilon_z|) = \begin{cases} 1 - \dfrac{D}{2R\alpha} + \dfrac{D^2}{12R^2\alpha^2} & \alpha > \dfrac{D}{2R} \\ \dfrac{2\alpha R}{3D} & 0 \leq \alpha \leq \dfrac{D}{2R}. \end{cases} \tag{28}$$

The analysis can now be completed as follows: we compute

$$P(|\epsilon_x| < |\epsilon_z|) = P\left(\left|\frac{1}{R} v\epsilon_z + \frac{-n_v + 1/2}{R}\right| < |\epsilon_z|\right)$$

$$\geq P\left(\frac{1}{R} v|\epsilon_z| + |B| < |\epsilon_z|\right) \tag{29}$$

$$= P\left(|B| < \left(1 - \frac{v}{R}\right)|\epsilon_z|\right) \tag{30}$$

using (26) and (27). Substituting into (28) gives the final result,

$$P(|\epsilon_x| < |\epsilon_z|) \geq \begin{cases} 1 - \dfrac{D}{2(R-v)} + \dfrac{D^2}{12(R-v)^2} & D < 2(R-v) \\ \dfrac{2(R-v)}{3D} & D \geq 2(R-v) \end{cases} \tag{31}$$

where we assume that $R > v$, as found in nearly all cases of practical interest.

*1) Experimental Verification:* To give evidence for the performance of the derived lower bound, a computer simulation of the stereo setup of Section IV provided 3-D points with image plane quantization noise. In particular the quantities $|\epsilon_x|$ and $|\epsilon_z|$ were calculated for points having disparities $D$ and vertical pixel offsets from center $v$, listed in Table I. For approximately 500 point samples for each row in Table I, $P(|\epsilon_x| < |\epsilon_z|)$ was calculated. This is compared to the bound computed from (31). From the results in Table I, the domination of the range error over the vertical error is made self evident. Note that the bounds, as expected, are fairly loose due to the use of the triangle inequality. Nonetheless, this rough estimate has been produced by avoiding the much more lengthy (and likely intractable) calculation of a joint distribution between the range and vertical errors.

TABLE I
PROBABILITY THAT RANGE ERROR $|\epsilon_z|$ EXCEEDS VERTICAL POSITION ERROR $|\epsilon_x|$

| v | D | R | Equation(31) | experiment |
|---|---|---|---|---|
| 10 | 50 | 376.27 | 0.933298 | 0.973643 |
| 80 | 50 | 376.27 | 0.917992 | 0.966434 |
| 150 | 50 | 376.27 | 0.893583 | 0.937500 |
| 220 | 50 | 376.27 | 0.848554 | 0.913105 |
| 10 | 80 | 376.27 | 0.894767 | 0.952966 |
| 80 | 80 | 376.27 | 0.871065 | 0.946479 |
| 150 | 80 | 376.27 | 0.833639 | 0.929825 |
| 220 | 80 | 376.27 | 0.765877 | 0.878650 |

### *E. Error in Range Dominates over Horizontal Position Error*

This section derives a lower bound for the probability that the error in the horizontal position is less than the error in range. This complements the discussion that began in the previous section in comparing the different positional error distributions; the last section was concerned with the vertical position error while the present section will derive an analogous expression for the horizontal error. The general approach will be the same in that the bound will arise from an application of the triangle inequality. However the intermediate expression differs substantially; all uncertainty in position arises from quantization in the horizontal ($J$) image coordinates due to the stereo setup (see Section IV).

We first express the horizontal position error in terms of the range error, horizontal image pixel offset, uncertainty parameters, and camera model constants as

$$\epsilon_y = (\hat{y} - y)/z = \frac{1}{R} h\epsilon_z + \frac{1}{R}(n_r - \tfrac{1}{2})$$

using (10) and (16). Letting $C \equiv 1/R\,(n_r - \frac{1}{2})$, a random variable on $[-1/2R, 1/2R]$, we now proceed as in the previous section observing that

$$|\epsilon_y| = \left|\frac{1}{R} h\epsilon_z + C\right|$$

$$\leq \frac{1}{R} h|\epsilon_z| + |C| \tag{32}$$

using the Triangle Inequality. To proceed further, it is

TABLE II
PROBABILITY THAT RANGE ERROR $|\epsilon_z|$ EXCEEDS HORIZONTAL POSITION ERROR $|\epsilon_x|$

| h | D | R | Equation(35) | experiment |
|---|---|---|---|---|
| 10 | 50 | 282.2 | 0.927363 | 0.936893 |
| 80 | 50 | 282.2 | 0.905422 | 0.911833 |
| 150 | 50 | 282.2 | 0.884609 | 0.829953 |
| 10 | 80 | 282.2 | 0.890247 | 0.896197 |
| 80 | 80 | 282.2 | 0.859578 | 0.881890 |
| 150 | 80 | 282.2 | 0.805538 | 0.800511 |

necessary to evaluate $P(\beta|C| \leq |\epsilon_z|)$ for some positive constant $\beta$. The details are omitted here for brevity considerations but can be found in Appendix D.

$$P(\beta|C| \leq |\epsilon_z|) = 1 - \frac{\beta D}{2(R + \beta D)} - \frac{\beta D}{16R}. \quad (33)$$

Returning to (32) we have

$$P(|\epsilon_y| < |\epsilon_z|) \geq P\left(\frac{1}{R} h|\epsilon_z| + |C| \leq |\epsilon_z|\right)$$
$$= P\left[\left(1 - \frac{h}{R}\right)^{-1} C \leq |\epsilon_z|\right]. \quad (34)$$

Replacing $\beta$ in (33) with the quantity multiplying $C$ in (34) gives

$$P(|\epsilon_y| < |\epsilon_z|) \geq 1 - \frac{D}{2(R - h) + D} + \frac{D}{16(R - h)} \quad (35)$$

where it is assumed that $R > h$, which is the case for most stereo setups of interest.

*1) Experimental Verification:* Analogous to (31), the above result was checked by performing a computer simulation using the stereo setup to simulate the quantization of the 3-D positional errors. Table II compares the experimentally determined probabilities to the bound calculated by (35). Each row of the table lists such a comparison for various combinations of disparity $D$ and horizontal pixel offsets $h$ for a fixed resolution factor $R = dv/f$. Examination of Table II reveals the extent to which range error dominates over error in the horizontal position. Also note that the bound derived in this section is somewhat tighter than that in Section V-D.

## V. SUMMARY AND DISCUSSION

This paper has quantified certain fundamental limitations in the accuracy of obtaining 3-D positional information based on triangulation of point correspondences derived from a stereo camera setup: the probability distributions of the errors in all three component directions have been derived and were given in (11), (18), and (25). A useful simplification to the range error cdf, (11), was given by (13) where the approximation was quantified by (14). Quantitative results relating the magnitudes of the vertical and horizontal errors to the range error have been presented, which were given by (31) for the former case and (35) for the latter. For all results discussed, the assumptions employed were rather general: in the absence of other information, a point's true 3-D position lies uniformly anywhere within a volume consistent with the image plane quantization. When measuring image position in terms of integral "image coordinates," the quantization in the image plane is clearly known. Alternatively, image position may be determined to subpixel accuracy by interpolating image feature positions. In this case, measurement errors are modeled by an appropriate spatial quantization at higher resolution. The imaging model was that of an ideal pinhole camera. Lens distortion and noise from electronic components have not been considered. Far from presenting an oversimplified error analysis, results obtained here are genuine upper bounds to performance of any such triangulation based system independent of the state of the current technology. Hopefully, the expressions obtained will have some impact on sensor design and synthesis. For computer image registration and tracking applications, the correlation between the different error components needed for estimation and filtering can be calculated based on the distributions derived here.

## APPENDIX A

Referring to Fig. 2, we can express the coordinates of the labeled points in the $y$–$z$ plane as

$$f_l = \left(-\frac{\Delta}{2}, f\right)$$
$$f_r = \left(+\frac{\Delta}{2}, f\right)$$
$$L_- = \left(-\frac{\Delta}{2} + (J_l - \tfrac{1}{2})\, dv, 0\right)$$
$$L_+ = \left(-\frac{\Delta}{2} + (J_l + \tfrac{1}{2})\, dv, 0\right)$$
$$R_- = \left(\frac{\Delta}{2} + (J_l - \tfrac{1}{2})\, dv, 0\right)$$
$$R_+ = \left(\frac{\Delta}{2} + (J_l + \tfrac{1}{2})\, dv, 0\right).$$

Also recall (2), the exact location of a point projected onto a horizontal line in the left image and right image planes. With (2) and the above defined quantities, the segment end points can be expressed as

$$P_5 = \left(\Delta\left(\frac{1}{2} + \frac{J_r + 1/2}{J_l - J_r + n_l - 1}\right), \frac{\Delta f}{(J_r - J_l + 1 - n_l)\, dv} + f\right)$$
$$P_6 = \left(\Delta\left(\frac{1}{2} + \frac{J_r + 1/2}{J_l - J_r + n_l}\right), \frac{\Delta f}{(J_r - J_l - n_l)\, dv} + f\right).$$

The segment $\overline{P5\ P6}$ (Fig. 2) can be shown to have length

$$\|P5 - P6\| = \frac{\Delta}{(J_1 - J_r + n_1)(J_1 - J_r + n_1 - 1)} \cdot \left[\frac{f^2}{dv^2} + (-J_1 - n_1 + \tfrac{1}{2})^2\right]^{1/2} \approx \frac{\Delta}{(J_1 - J_r + n_1)(J_1 - J_r + n_1 - 1)} \cdot \left[\frac{f^2}{dv^2} + J_1^2\right]^{1/2} \quad \text{(A1)}$$

since, if $J_1$ is large, $n_1 \ll J_1$. Otherwise, the $f^2/dv^2$ term dominates regardless of the value of $n_1$. It can be further established that

$$P_7 = \left(\Delta\left(\frac{1}{2} + \frac{J_r + n_r - 1}{J_1 - J_r + n_1 - n_r}\right), \frac{\Delta f}{(J_r - J_1 + n_r - n_1)\, dv} + f\right)$$

and that

$$P_8 = \left(\Delta\left(\frac{1}{2} + \frac{J_r + n_r + dn_r - 1}{J_1 - J_r + n_1 - n_r - dn_r}\right), \frac{\Delta f}{(J_r - J_1 + n_r + dn_r - n_1)\, dv} + f\right).$$

The length of the projection of an infinitesimally thin interval of width $dn_r$ in the image plane upon segment $\overline{P5\ P6}$ can be shown to be

$$\|P7 - P8\| = \Delta\left[\frac{dn_r}{(J_1 - J_r + n_1 - n_r - dn_r)} - \frac{dn_r}{(J_1 - J_r + n_1 - n_r)}\right] \cdot \left[\frac{f^2}{dv^2} + (-J_1 - n_1 + \tfrac{1}{2})^2\right]^{1/2} \approx \Delta\left[\frac{dn_r}{(J_1 - J_r + n_1 - n_r - dn_r)} - \frac{dn_r}{(J_1 - J_r + n_1 - n_r)}\right] \cdot \left[\frac{f^2}{dv^2} + J_1^2\right]^{1/2}$$

under the same approximation made earlier. Expanding the leftmost square-bracketed term in the above expression into a Taylor series and retaining the second order terms, it turns out that a cancellation with a negative term of $\|P7 - P8\|$ occurs, giving

$$\|P7 - P8\| \approx \frac{\Delta dn_r^2}{(J_1 - J_r + n_1 - n_r)^2}\left[\frac{f^2}{dv^2} + J_1^2\right]^{1/2}.$$

Since $dn_r^2$ can be made arbitrarily small compared to the rest of the quantities defined in the above expression, $dn_r$ can be redefined as $dn_r' \equiv dn_r^2$, finally yielding

$$\|P7 - P8\| \approx \frac{\Delta dn_r'}{(J_1 - J_r + n_1 - n_r)^2}\left[\frac{f^2}{dv^2} + J_1^2\right]^{1/2}. \quad \text{(A2)}$$

## Appendix B

To determine how closely (13) approximates (11), we will derive an upper bound on the maximum $L^1$ distance between the two functions. For the purposes of this discussion we will assume that $D > 1$. Let

$$\xi \equiv \left|\ln(1 - \tau_z^2) - (-\tau_z^2)\right| < \frac{1}{2}\left(\sum_{n=2}^{\infty}(\tau_z^2)^n\right) = \frac{\tau_z^4}{2(1 - \tau_z^2)} \le \frac{\tau_z^4}{2} \quad \text{(B1)}$$

where the first inequality is obtained by expressing the logarithm as a Taylor series expansion about zero. We similarly let

$$\delta \equiv \left|\ln(1 - D^{-2}) - (-D^{-2})\right| < \frac{1}{2(D^4 - 1)}. \quad \text{(B2)}$$

We first note that (11) and (13) are identically equal to one for $\tau_z \ge D^{-1}$. For all $\tau_z < D^{-1}$, $\zeta < (1/2D^4) < \delta$ using (B1). Thus, we see that the maximum error in (11) over all $\tau_z$,

$$\operatorname*{argmax}_{\tau_z}\left|P_{|\epsilon_z|}(\tau_z) - \hat{P}_{|\epsilon_z|}(\tau_z)\right| \le \operatorname*{argmax}_{\tau_z}\left|\frac{k_1 + k_2 + \xi}{k_3 - \delta} - \frac{k_1 + k_2 - \xi}{k_3 + \delta}\right| \quad \text{(B3)}$$

$$< \operatorname*{argmax}_{\tau_z}\left|\frac{k_1 + k_2 + \delta}{k_3 - \delta} - \frac{k_1 + k_2 - \delta}{k_3 + \delta}\right| \quad \text{(B4)}$$

where

$$k_1 \equiv -\frac{2\tau_z(\tau_z - D^{-1})}{1 - \tau_z^2} \quad \text{(B5b)}$$

$$k_2 \equiv -\ln(1 - \tau_z^2)$$

$$k_3 \equiv -\ln(1 - D^{-1}) \quad \text{(B5c)}$$

since $(k_1 + k_2)/k_3 > 0$ and $k_3 > \delta$. Simplifying (B4),

$$\operatorname*{argmax}_{\tau_z}\left|P_{|\epsilon_z|}(\tau_z) - \hat{P}_{|\epsilon_z|}(\tau_z)\right| < \operatorname*{argmax}_{\tau_z}\frac{2\delta(k_1 + k_2)}{k_3^2 - \delta^2} \le \operatorname*{argmax}_{\tau_z}\frac{2\delta(k_1 + k_2)}{k_3^2} = \operatorname*{argmax}_{\tau_z}\frac{2\delta}{k^3}\left(\frac{k_1 + k_2}{k_3}\right). \quad \text{(B6)}$$

But $(k_1 + k_2)/k_3 \leq 1$ since it is identical to (11), a probability distribution function, which implies

$$\operatorname{argmax}_{\tau_z} \left| P_{|\epsilon_z|}(\tau_z) - \hat{P}_{|\epsilon_z|}(\tau_z) \right| < \frac{2\delta}{k_3} \leq \frac{D^2}{D^4 - 1} \quad \text{(B7)}$$

where we have substituted (B5c) and (B2) to get the last inequality, and noted that $D^{-2}$ is larger than $k_3$.

## Appendix C

Examining the quantity $B$ in Section V-D in view of the assumptions in Section IV, it is obvious that the vertical ($x$) position of the point in 3-D projects onto the ($I$) coordinate in each image plane with uniform distribution. Moreover, the $I$ coordinate, $I_l + n_{l'} - \frac{1}{2}$, is the same in each image and is independent of the horizontal projections $n_r$ and $n_l$. The density for the quantity $B$ is just that of $n_{l'}$ scaled by the factor $2R$ and shifted by $\frac{1}{2}$:

$$f_B(b) = \begin{cases} R & -\dfrac{1}{2R} < b < \dfrac{1}{2R} \\ 0 \cdot & \text{otherwise.} \end{cases}$$

The density of the error in range, $T_z = |\epsilon_z|$, is the derivative of its cdf, approximated by (13), or

$$f_{T_z}(\tau_z) = \begin{cases} 2(D - D^2\tau_z) & \tau_z < D^{-1} \\ 0 & \tau_z \geq D^{-1}. \end{cases}$$

Since the random variables $T_z$ and $B$ are independent,

$$f_{B,T_z} = f_{T_z} f_B. \quad \text{(C1)}$$

$P(|B| \leq \alpha |\epsilon_z|)$ is obtained by integrating (C1) in the appropriate region:

$$\begin{aligned} P(|B| \leq \alpha|\epsilon_z|) &= \int_{\alpha T_z > |B|} \int f_{T_z}(\tau_z) f_B(b)\, db\, d\tau_z \\ &= 2 \int_0^{\tau_z/2\alpha R} \int_0^{\tau_z \alpha} 2R(D - D^2\tau_z)\, db\, d\tau_z \\ &\quad + 2 \int_{\tau_z/2R\alpha}^{1/D} \int_0^{1/2R} 2R(D - D^2\tau_z)\, db\, d\tau_z \\ &= \begin{cases} 1 - \dfrac{D}{2R\alpha} + \dfrac{D^2}{12R^2\alpha^2} & \alpha > \dfrac{D}{2R} \\ \dfrac{2\alpha R}{3D} & 0 \leq \alpha \leq \dfrac{D}{2R}. \end{cases} \end{aligned} \quad \text{(C2)}$$

## Appendix D

In this section, we will evaluate $P(\beta|C| \leq |\epsilon_z|)$ for some positive constant $\beta$. From (10) and the definition of $C$ in Section V-E,

$$\begin{aligned} P(\beta|C| \leq |\epsilon_z|) &= P\left(\frac{\beta|n_r - 1/2|}{R} \leq \frac{|n_r - n_l|}{D}\right) \\ &= P\left(n_l < n_r\left(1 - \frac{\beta D}{R}\right) + \frac{1}{2R}\right) \\ &\qquad n_r > \frac{1}{2},\ n_r > n_l \\ &= P\left(n_l > n_r\left(1 - \frac{\beta D}{R}\right) - \frac{1}{2R}\right) \\ &\qquad n_l > n_r > \frac{1}{2} \\ &\quad P\left(n_l < n_r\left(1 + \frac{\beta D}{R}\right) - \frac{1}{2R}\right) \\ &\qquad n_l < n_r < \frac{1}{2} \\ &\quad P\left(n_l > n_r\left(1 - \frac{\beta D}{R}\right) + \frac{1}{2R}\right) \\ &\qquad n_r < \frac{1}{2},\ n_r < n_l. \end{aligned} \quad \text{(D1)}$$

Interpreting the $n_r - n_l$ plane geometrically, it is quite easily shown that (D1) is a sum of four nonoverlapping regions corresponding to the four regions above. With the approximation of Section V-A-2), the four cases can be interpreted geometrically as the areas of four bounded regions in the $n_r - n_l$ plane. This leads to the evaluation of the following:

$$\begin{aligned} P(\beta|C| \leq |\epsilon_z|) &= \int_{1/2}^{1} \int_0^{n_r(1-\beta D/R)+1/2R} dn_l\, dn_r \\ &\quad + \int_{1/2}^{(2R+1)/2(R+\beta D)} \int_{n_r(1+\beta D/R)-1/2R}^{1} dn_l\, dn_r \\ &\quad + \int_{1/2\beta D}^{1/2} \int_{1/2\beta D}^{n_r} dn_l\, dn_r \\ &\quad + \int_0^{1/2\beta D} \int_{n_r(1+\beta D/R)-1/2R}^{1/2} dn_l\, dn_r \\ &\quad + \int_{1/2\beta D}^{1/2} \int_{n_r}^{1} dn_l\, dn_r \\ &\quad + \int_0^{1/2\beta D} \int_{n_r(1-\beta D/R)+1/2R}^{1} dn_l\, dn_r \\ &= 1 - \frac{\beta D}{2(R + \beta D)} - \frac{\beta D}{16R}. \end{aligned} \quad \text{(D2)}$$

## REFERENCES


[1] S. Barnard and M. A. Fischler, "Computational stereo," *Comput. Surveys*, vol. 14, no. 4, Dec. 1982.

[2] E. S. McVey and J. W. Lee, "Some accuracy and resolution aspects of computer vision distance measurements," *IEEE Trans. Pattern Anal. Machine Intell.*, vol. PAMI-4, pp. 646–649, Nov. 1982.

[3] K. Drake, E. S. McVey, and R. M. Inigo, "Sensing error for a mobile robot using line navigation," *IEEE Trans. Pattern Anal. Machine Intell.*, vol. PAMI-7, pp. 485–490, July 1985.

[4] S. D. Blostein, "Motion estimation based on stereo sequences," M.S. thesis, Univ. Illinois at Urbana-Champaign, May 1985.

[5] N. Ayache, O. D. Faugeras, B. Faverson, and G. Toscani, "Matching depth maps obtained by passive stereo," in *Proc. Third Workshop Computer Vision: Representation and Control*, Bellaire, MI, Oct. 1985.

[6] D. Terzopoulos, "Multilevel computational processes for visual surface reconstruction," *Comput. Vision, Graphics, Image Processing*, vol. 24, pp. 52–96, 1983.

[7] H. P. Moravec, "Rover visual obstacle avoidance," in *Proc. 7th Int. Joint Conf. Artificial Intelligence*, vol. 2, Vancouver, Aug. 1981, pp. 785–790.

[8] R. A. Jarvis, "A perspective on range finding techniques for computer vision," *IEEE Trans. Pattern Anal. Machine Intell.*, vol. PAMI-5, No. 2, Mar. 1983.

[9] A. C. Kak, "Depth perception for robots," Purdue Univ., Tech. Rep. TR-EE-83-44, 1983.

[10] D. B. Gennery, "Object detection and measurement using stereo vision," in *Proc. Image Understanding Workshop*, College Park, MD, Apr. 1980, pp. 161–167.

[11] J. B. Thomas, *An Introduction to Applied Probability and Random Processes*. New York: Kreiger, 1971.

[12] R. Duda and P. Hart, *Pattern Classification and Scene Analysis*. New York, 1973.

[13] Y. Yakimovsky and R. Cunningham, "A system for extracting three-dimensional measurements from a stereo pair of TV cameras," *Comput. Graphics, Vision, Image Processing*, vol. 7, pp. 195–210, 1978.

[14] *Manual of Photogrammetry*, 3rd ed., Amer. Soc. Photogrammetry, 1966.

[15] F. Solina, "Errors in stereo due to quantization," Univ. Pennsylvania, Tech. Rep. MS-CIS-85-34, Sept. 1985.

[16] A. Verri and V. Torre, "Absolute depth estimates in stereopsis," *J. Opt. Soc. Amer.*, vol. 3, no. 3, pp. 297–299, Mar. 1986.

[17] O. D. Faugeras, N. Ayache, and B. Faverjon, "Building visual maps by combining noisy stereo measurements," in *Proc. 1986 IEEE Robotics and Automation Conf.*, pp. 1433–1438.


**Steven D. Blostein** (S'83) was born in Urbana, IL, on April 1, 1961. He received the B.S. degree in electrical engineering from Cornell University, Ithaca, NY, in 1983, and the M.S. degree in electrical and computer engineering from the University of Illinois, Urbana-Champaign, in 1985, where he is currently working toward the Ph.D. degree.

During his undergraduate years he was employed by Canadian Marconi Company as a cooperative work student, and by Bell Northern Research in Montreal, Canada, as a summer student. During 1983–1984 he was a Teaching Assistant for the Department of Electrical and Computer Engineering, University of Illinois. Since then, he has been employed by the Coordinated Science Laboratory, University of Illinois, as a Research Assistant. He has also performed consulting work for industry and government. His current interests are in signal and image processing, detection and estimation, and computer vision: in particular, the application of nonlinear statistical methods to image analysis and pattern recognition.

Mr. Blostein is a member of Eta Kappa Nu.

**Thomas S. Huang** (S'61–M'63–SM'76–F'79) received the B.S. degree in electrical engineering from National Taiwan University, Taipei, Taiwan, China, and the M.S. and Sc.D. degrees in electrical engineering from the Massachusetts Institute of Technology, Cambridge.

He was on the Faculty of the Department of Electrical Engineering at M.I.T. from 1963 to 1973, and on the Faculty of the School of Electrical Engineering and Director of its Laboratory for Information and Signal Processing at Purdue University from 1973 to 1980. In 1980, he joined the University of Illinois at Urbana-Champaign, where he is now Professor of Electrical and Computer Engineering and Research Professor at the Coordinated Science Laboratory. During his sabbatical leaves, he has worked at the M.I.T. Lincoln Laboratory, the IBM Thomas J. Watson Research Center, and the Rheinishes Landes Museum in Bonn, West Germany, and held visiting Professor positions at the Swiss Institutes of Technology in Zürich and Lausanne, University of Hannover in West Germany, and INRS-Telecommunications of the University of Quebec in Montreal, Canada. He has served as a consultant to numerous industrial firms and government agencies both in the U.S. and abroad. His professional interests lie in the broad area of information technology, especially the transmission and processing of multidimensional signals. He has published 10 books, and over 200 papers in network theory, digital filtering, image processing, and computer vision.

Dr. Huang is a Fellow of the Optical Society of America and has received a Guggenheim Fellowship (1971–1972), an A. V. Humboldt Foundation Senior U. S. Scientist Award (1976–1977), and a Fellowship from the Japan Association for the Promotion of Science (1986). He is an Editor of the international journal *Computer Vision, Graphics, and Image Processing*, Editor of the *Springer Series in Information Sciences*, published by Springer Verlag, and Editor of the *Research Annual Series on Advances in Computer Vision and Image Processing* published by JAI Press.

## References

[1] G. T. Toussaint, "Movable separability of sets," in *Computational Geometry*, G. T. Toussaint, Ed. Amsterdam, The Netherlands: North-Holland, 1985, pp. 335–375.

[2] M. I. Shamos, "Computational geometry," Ph.D. dissertation, Yale Univ., 1978.

[3] K. Q. Brown, "Geometric transforms for fast geometric algorithms," Dep. Comput. Sci., Carnegie-Mellon Univ., 1979.

[4] D. G. Kirkpatrick and R. Seidel, "The ultimate planar convex hull algorithm?", Dep. Comput. Sci., Cornell Univ., Tech. Rep. 83-577, Oct. 1982.

[5] M. M. McQueen and G. T. Toussaint, "On the ultimate convex hull algorithm in practice," *Pattern Recognition Lett.*, pp. 29–34, Jan. 1985.

[6] D. McCallum and D. Avis, "A linear time algorithm for finding the convex hull of a simple polygon," *Inform. Processing Lett.*, pp. 201–205, Dec. 1979.

[7] D. T. Lee, "On finding the convex hull of a simple polygon," Tech. Northwestern Univ., Tech. Rep. 80-03-FC-01, Mar. 1980.

[8] L. Guibas and R. Seidel, "Computing convolutions by reciprocal search," in *Proc. 2nd Symp. Comput. Geom.*, Yorktown Heights, NY, 1986, pp. 90–99.

[9] M. E. Houle and G. T. Toussaint, "Computing the width of a set," Tech. Rep. SOCS-84.22, Dec. 1984.

[10] F. P. Preparata and S. J. Hong, "Convex hulls of finite sets of points in two and three dimensions," *Commun. ACM*, vol. 20, pp. 87–93, 1977.

[11] K. Ichida and T. Kiyono, "Segmentation of plane curves," *Trans. Elec. Commun. Eng., Japan*, vol. 58-D, pp. 689–696, 1975.

[12] H. Imai and M. Iri, "Polygonal approximations of a curve: Formulations and solution algorithms," in *Computational Morphology*, G. T. Toussaint, Ed. Amsterdam, The Netherlands: North-Holland, to be published.

[13] Y. Kurozumi and W. A. Davis, "Polygonal approximation by the minimax method," *Comput. Graphics Image Processing*, vol. 19, pp. 248–264, 1982.

[14] G. Toussaint, "Solving geometric problems with the rotating calipers," in *Proc. MELECON '83*, Athens, Greece, 1983.

[15] G. Toussaint, "Approximating polygonal curves in three-dimensions," manuscript in preparation.


## Correction to "Error Analysis in Stereo Determination of 3-D Point Positions"

STEVEN D. BLOSTEIN AND THOMAS S. HUANG

In the above paper[1] algebraic errors were introduced in the final algebraic simplification of Equations (18) and Equation (25) for presentation purposes. However, the plotted graphs of these expressions, i.e., Figs. 5 and 6, are correct. In Equation (18), the term $B - A \operatorname{sgn}(h - D)$ should be replaced by $B + [2DRt_y/(h - D)] \operatorname{sgn}(h - D)$. In Equation (25), the "$D \geq v$" case should read

$$\begin{cases} 1 & t_x > \dfrac{v}{DR} + \dfrac{1}{2R} \\ \phi + \psi + 1/2 & \dfrac{1}{2R} < t_x \leq \dfrac{v}{DR} + \dfrac{1}{2R} \\ \phi - \psi + 1/2 & \left| -\dfrac{v}{DR} + \dfrac{1}{2R} \right| < t_x \leq \dfrac{1}{2R} \\ 2Rt_x & 0 \leq t_x \leq \dfrac{1}{2R} - \dfrac{v}{DR} \quad \text{and} \quad D \geq 2v \\ \rho & 0 \leq t_x \leq \dfrac{v}{DR} - \dfrac{1}{2R} \quad \text{and} \quad D < 2v. \end{cases}$$

The authors gratefully acknowledge B. Kamgar-Parsi, University of Maryland, for pointing out these errors.

Manuscript received June 27, 1988. Recommended for acceptance by W. B. Thompson.

The authors are with the Coordinated Sciences Laboratory, University of Illinois, 1101 West Springfield Ave., Urbana, IL 61801.

IEEE Log Number 8823187.

[1] S. D. Blostein and T. S. Huang, *IEEE Trans. Pattern Anal. Machine Intell.*, vol. PAMI-9, no. 6, pp. 752–765, Nov. 1987.